Results in Earth Sciences 1 (2023) 100002

Contents lists available at ScienceDirect

Results in Earth Sciences

journal homepage: www.sciencedirect.com/journal/results-in-earth-sciences

Morphotectonics and paleostress analyses of Kutch area, Gujarat, India

Mayur Shashikant Dhawale[a], Soumyajit Mukherjee[b,*], Mery Biswas[c]

[a] Department of Earth and Climatic Science, Indian Institute of Science Education and Research, Dr. Homi Bhabha Road, Pashan, Pune 411008, Maharashtra, India
[b] Department of Earth Sciences, Indian Institute of Technology Bombay, Powai, Mumbai 400076, Maharashtra, India
[c] Department of Geography, Presidency University, 86/1 College Street, Kolkata 700073, West Bengal, India

ARTICLE INFO

Keywords:
Deformation mechanism
Plate tectonics
Geodynamics
Rift basin
Basin tectonics

ABSTRACT

The Kutch Rift Basin (KRB) is of great attention for its possible hydrocarbon reserve. In this context, geomorphologic and structural geologic studies of the onland basin area are crucial. Application of geomorphic indicators viz., compactness coefficient (Cc), lemniscate coefficient (k), form ratio (Rf), basin shape index (Bs), basin asymmetry factor (AF), hypsometric integral (HI), elongation ratio (Re) and circularity ratio (Rc) have been utilized to calculate the Index of Active Tectonics (IAT) for a part of KRB. Watersheds 5 (the Bhuj area), 9, 10, 11, 17, 18 and 20 belong to class 1 as per the IAT. This indicates that these watersheds are very highly tectonically active at present. Calculated valley floor width height ratio (V_f) and mountain front sinuosity (Smf) quantify the active valley incision in the Quaternary that uplifted the Bhuj area. This uplift was accompanied by a high-degree of drainage rejuvenation due to neotectonics and formation of a canyon in the Khari river. Paleostress analyses revealed NNE and NW-oriented extensions around Bhuj that can correspond to NW and NNE-trending normal fault planes, respectively.

1. Introduction

Tectonic geomorphology and structural geologic analyses of rift basins (e.g., Dasgupta and Mukherjee, 2017, 2019; Dasgupta et al., 2022) are of global attention. Such geoscientific studies attain more importance when the basin is petroliferous. The Kutch/ Kachchh basin in the Indian western offshore region has been well known for a long time for its possible hydrocarbon prospect (e.g., review in Dwivedi, 2016) and therefore has been studied intensely geophysically and geologically (e.g., Sen et al., 2019). Recent discovery of hydrocarbon from the Kutch onshore area has promoted geoscientists to re-look at the terrain (internet ref 1, 2). Interestingly, geochemical studies from sub-surface rocks samples proved that the Bhuj area (along with the locations Anjar, Mandavi and Mundra) can have thermogenic hydrocarbon at some depth (Patil et al., 2013).

Thakkar et al. (1999) reported the geomorphology around Bhuj and provided a four-fold geomorphic classification of the Kutch region. The authors referred to meandering to river patterns around the location of the Bhuj. Patidar et al. (2007) reported an abnormally deep and unique incised river channel near Bhuj, which is uncommon in the nearby areas. Sandstone crops out as a uniform lithology around Bhuj, and the typical geomorphology-gentle slopes, low relief, dendritic drainage. Tilting due to morpho-dynamics have been worked out quantitatively (Alapati et al., 2019).

While some amount of geomorphic information from places around Bhuj is available, meso-scale structural data is especially sparse. For example, only Morino et al. (2008) identified ~ NE-trending Bhuj Fault based on fieldwork and remote sensing images.

Omid et al. (2021) documented three or more generations of quartz veins from the Bhuj sandstone. Lohani et al. (2022) presented a structural geologic field guide from the Bhuj and nearby areas, mostly covering the Katrol Hill Range Fault Zone.

This article presents *(i)* morpho-tectonic analyses of geomorphic features from the Kutch, and (ii) detailed paleostress analyses from the sandstone exposures around Bhuj. Performing smaller-scale paleostress studies in the regional geoscientific context is a standard practice in geoscience (e.g., Shaikh et al., 2018).

2. Geology, geomorphology and tectonics

The tectonic evolution and the shape of the pericratonic palaeorift Kutch basin is a result of the break-up of the Indian plate at its western margin from the Gondwanaland (Mukherjee et al., 2020). This was followed by a rapid northward drift of the Indian plate resulting in the collision with the Eurasian plate ~ 55 Ma back (Goswami et al., 2020). Several faults generated by the breakup were reactivated during the later collision (Dasgupta and Mukherjee, 2017) (Fig. 1A-B). Such reactivation has been reported from several regional faults in the KRB

* Corresponding author.
E-mail addresses: soumyajitm@gmail.com, smukherjee@iitb.ac.in (S. Mukherjee).

https://doi.org/10.1016/j.rines.2023.100002
Received 28 June 2023; Received in revised form 14 August 2023; Accepted 25 August 2023

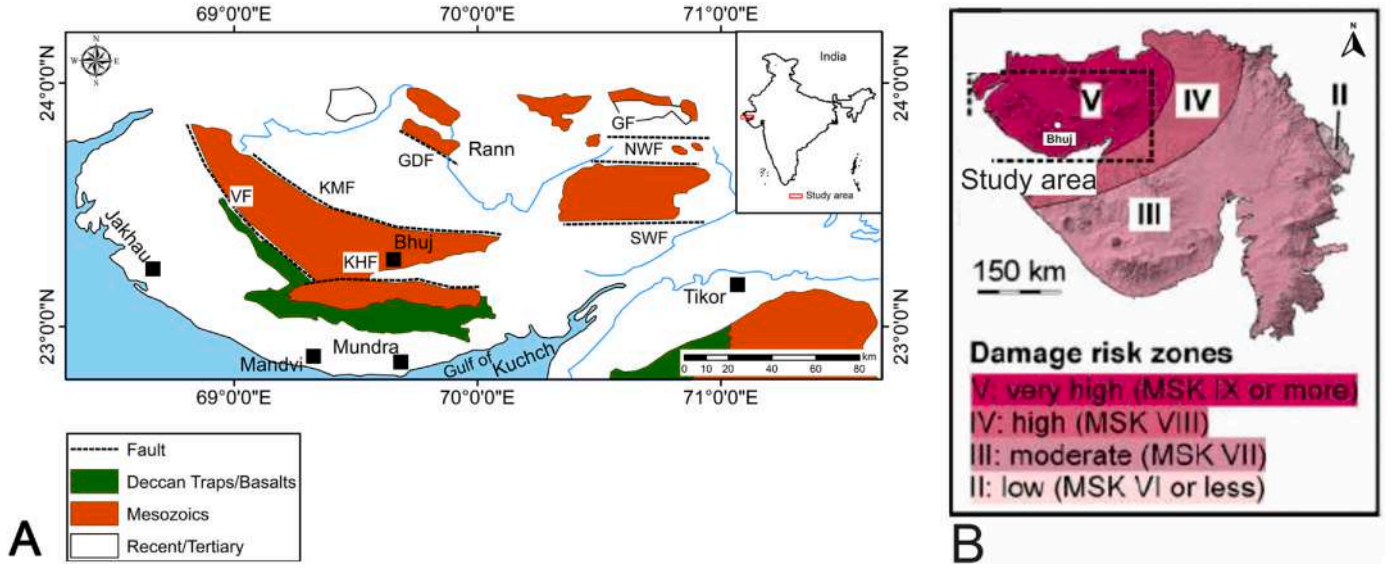

Fig. 1. A. The Kutch basin (reproduced from Seshu et al., 2016 where Bhuj is shown. KMF: Kutch Mainland Fault, KHF: Katrol Hill Fault, VF: Vigodi Fault, SWF: South Wagad Fault, NWF: North Wagad Fault, GF: Gedi Fault, GDF: Gora Dongar Fault. B. Seismic zones marked in the state Gujarat (after Shaikh et al., 2020). Study area marked.

(Mukherjee, 2018). The recent earthquake history around Bhuj (and Saurashtra) also suggests an active tectonic regime (e.g., Vanik et al., 2018; Shaikh et al. 2022). Uplift rate of the KRB ranges from 0.8 up to 2.8 mm yr^{-1} (Jani et al. 2021; Kothyari et al. 2022).

The tectonic landscape of the KRB is characterized by the Mainland uplift, Wagad uplift, Desalpar uplift and the Island Belt uplift. In the Cretaceous Period, the basin was inverted, whereby prior normal faults activated as reverse faults (review in Chandrasekhar et al., 2012), and formed the intra-basinal uplifts with respect to the structural lows (Biswas and Khattri, 2002). During post-Cretaceous inversion, flexing further modified the topography. Later, a thin Quaternary sediment layer was deposited on Katrol Hill (Chowksey et al., 2011a, 2011b). The entire area is drained by rivers and their tributaries flowing S-N, N-S, E-W and W-E originating from the W-E anticlinal ridge forming meso to micro-scale watersheds. These watersheds modified slopes due to tectonics (Singh, 2014; Withanage et al., 2014). With time, drainage system

Table 1
Detail methodology for characterizing relief, drainage and channel morpho-geometry.

Sl no.	Indices	Relief Characterizes	Reference
1.	Absolute Relief map	Extracted from DEM in Arc GIS10.3	*NA*
2.	Aspect Map	Extracted from DEM in Arc GIS10.3	*NA*
3.	Slope map	Extracted from DEM in Arc GIS10.3	
Sl. No.	**Indices**	**Drainage Analysis**	**Reference**
1.	Drainage Pattern	Extracted from Drainage map.	Morisawa (1985)
Sl. No.	**Indices**	**Geometric and morphometric Parameters**	**Reference**
1.	Compactness co-efficient(Cc)	$Cc = \frac{P_B}{\sqrt{4\pi A_B}}$ Here P_B is the perimeter of the basin and A_B is the area of the same basin. A tectonically active basin will have a higher Cc value and vice-versa.	e.g.Iqbal and Sajjad (2014)
2.	Form ratio(Rf)	$R_f = \frac{A_B}{(L_b)^2}$ Here Form ratio (R_f), ratio of the basin area (A_B)to the square of its length (L_b)	e.g.,Paul and Biswas (2019);Kale et al., (2014)
3.	Lemniscate coefficient(k)	$k = \frac{\pi L_b^2}{4A_B}$ Here, A_B is the area of basin and L_b is the length of the basin.	
4.	Basin Shape Index (Bs)	$Bs = \frac{L_b}{W_b}$ Here Length (L_b) to the width of the basin at its wisest part (W_b).	Chorley (1957) e.g.Anand and Pradhan (2019)
5.	Basin Asymmetry Factor(AF)	$Basin\ Asymmetry\ Ratio = \frac{A_r}{A_t} \times 100$ Here A_r is the area of basin to the right of the stream flowing downstream and A_t is the total area of the entire basin. When this value is nearer to 50, the basin is supposed to be tectonically inactive, while as the value go away from 50 (0–35 and 65–100). For IAT Normalized Basin Asymmetry Ratiois obtained.	e.g.Anand and Pradhan (2019)
6.	Hypsometric Integral (HI)	$HI = \frac{(Hmean - H\ min)}{(H\ max - H\ min)}$ Here Hmean= Mean Elevation Hmin= Minimum Elevation Hmax= Maximum Elevation	Strahler (1952),Schumm (1956), Chen et al., (2003) e.g.Anand and Pradhan (2019)
7.	Elongation ratio (Re)	$Re = 1.128\sqrt{A} * Lb$ Here, Lb= Length of the basin A= Area of the river basin	e.g.Anand and Pradhan (2019)
8.	Circularity ratio(Rc)	$Rc = 4\pi A/P^2$ Here, A= Area of the basin P = Perimeter of the basin	e.g.Anand and Pradhan (2019)
9.	Sinuosity Index (SI)	$SI = \frac{\text{Channel Length}}{\text{Valley length}}$ Here, Straight channel values < 1.05 Straight to Sinuous values between > 1.05 - < 1.50 Meandering channel indicates > 1.50	Brice (1964), e.g.Biswas and Dhara, (2019)

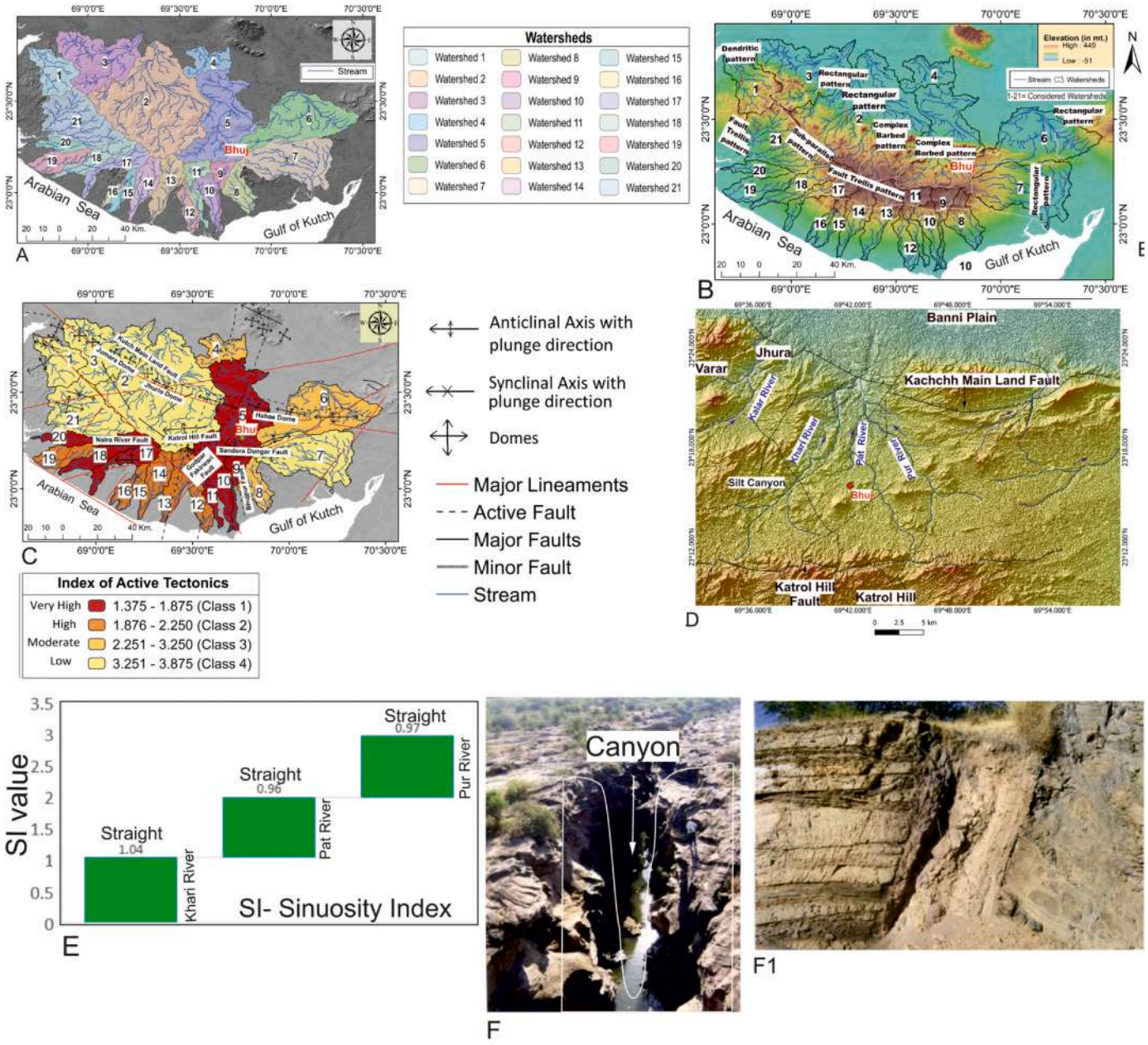

Fig. 2. A. Delineated 21 watersheds of Bhuj and its surrounding area. Watersheds are multidirectional as per the regional slope. Extracted from SRTM 30 m resolution 2015 data. B. Drainage patterns developed over the watersheds indicate the drainage network and structural control. C. Map of computed Index of Active Tectonics where seven watersheds are under class 1, six under class 2, three under class 3, and five under class 4 watersheds. The map is overlain by faults and lineaments along with anticlinal and synclinal axes. Faults e.g., KMF, Naira river fault, KHF, Godpar Fakirwari fault, Bhujpur fault, Sandsra Dungar fault are shown. D. Micro-level study of watershed 5 (tectonically active) with reverse fault, and active faults where three individual rivers are characterized by structural control. E. Computed SI values of the Khari, Pat and Pur rivers. All are straight channels indicating vertical incision stronger than lateral erosion. F. I-shaped canyon in the Khari River. F1. Photo evidence of the Kutch Shear Zone (after Valdiya and Sanwal, 2017).

adjusted to local structures such as faults and lineaments and acquired typical valley incision geometry, basin shape, asymmetry, stream length gradient, sinuosity etc. (Prakash et al., 2017; Biswas and Paul, 2021).

The Kutch region is characterized by four geomorphologic zones: *(i)* Great Rann in the north and Little Rann in the western part, *(ii)* Banni-Plains or Rann segment, *(iii)* rocky upland in the Kutch Mainland, and *(iv)* southern fringe of curved coastal littoral section (Malik et al., (2001)). Anticline, monocline flexure, and W-E striking Kutch Mainland Fault reoriented the drainage pattern in response to the fluvial interaction.

This study section of the KRB is a part of the rocky upland. This article uses the terms 'watersheds' and 'river basins', which are the same in the context of their linear and spatial analyses (e.g., Biswas et al., 2022; Dasgupta et al., 2022). This article uses the parameters *"basin shape index"*, and *"basin asymmetry"* on the defined watersheds for which it was necessary to clarify this point.

3. Methods

3.1. Morphotectonic parameters

Integrated morpho-tectonic analyses were performed and data were computed using Digital Elevation Model (DEM). The DEM data consist of SRTM 30 m resolution of Tile Downloader in EOSDIS Earth data of

National Aeronautics and Space Administration (NASA). It is a zipped SRTMHGT file at 1-arcsecond resolution (3601 ×3601 pixels) in a latitude/longitude projection (EPSG: 4326).

Using the fill DEM to flow accumulation through stream feature class criteria, twenty-one watersheds have been identified in the ARC GIS 3.4 platform (2016). The extracted surface terrain model calculates slope, creates aspect maps and helps to delineate the watersheds. Drainage lines are enhanced to calculate the parameters of the individual watersheds. Q-GIS 3.12 platform has been used to prepare the 3D layout of the area on which major faults (Kutch Mainland Fault, Katrol Hill Fault, Naira River Fault, Sandra Dungar Fault, Bhujpur Fault and Godpar Fakirwari Fault) were overlaid from the literature. Maps are georeferenced and faults are plotted on the 3D terrain map. Draping of data was avoided in the DEM. We have used an advanced technique (Kumar et al., 2018) that gives results of different considered morphotectonic parameters. We can compare tectonic set-up, lithology, geomorphic features and channel characteristics.

For the critical analysis of these parameters, mountain front sinuosity (Smf) and valley floor width to height ratio (V_f) were calculated and classified into four classes by separately considering the same spatial entity. Further, we compared the Index of Active Tectonics (IAT) in response of uplift rate and existence of fault lines. This leads to tectonically relevant conclusions (as in Kumar et al., 2018).

The tectonically active watersheds are assessed using the IAT. Computed IATs provide a reliable semi-quantitative measure of tectonic activeness in a relative sense (e.g., Bull and McFadden, 1977; Gupta and Biswas, 2022). We evaluate relative active tectonics based on seven measures such as compactness coefficient (Cc), lemniscate coefficient (k), form ratio (Rf), basin shape index (Bs), basin asymmetry factor (AF), hypsometric integral (HI), elongation ratio (Re) and circularity ratio (Rc) (Table 1). All the values of the considered parameters have been classified into four classes (1 − 4). These parameters taken together enable computing the IAT. This led to categorizing the watersheds with low, moderate, high and very high tectonic activities.

To assess the relative tectonic activity, the Smf index has frequently been used (Bull and McFadden, 1977; El Hamdouni et al., 2008). This parameter indicates equilibrium in tectonic uplift, which helps to produce irregular fronts. Smf is defined as follows (Bull and McFadden, 1977; Bull, 2007):

$$Smf = \frac{Lmf}{Ls} \quad (1)$$

Here Lmf: overall planimetric length of a mountain front along the mountain and piedmont junction, and Ls: length of this front's straight line.

The V_f ratio is defined as (Bull and McFadden, 1977):

$$Vf = \frac{2Vfw}{[(Eld - Esc) + (Erd - Esc)]} \quad (2)$$

Here V_f w is the width of the valley floor, Eld and Erd are the elevations of the divide on the left and right side of the valley, respectively. Esc is the average elevation of the valley.

This ratio is connected to an incision and indicates active tectonics due to uplift. Low values of V_f related to V-shaped valleys may be related to tectonic uplift-induced vertical incision (Sahu and Mohanty, 2021). High values of V_f for the U-shaped valley connote lateral erosion primarily due to dormant relative tectonic. In this study, 63 points from 21 watersheds have been considered and sequentially two points are taken-one from upstream mountain front and the other from the downstream portion.

3.2. Structural and paleostress studies

Fault planes and slickenlines were documented from five locations around Bhuj within the Bhuj Sandstones. Other meso-scale faults were noted and many of them were not incorporated into paleostress studies because of the lack of development of tectonic lineations over them. The collected data from each sector is presented in the Repository Tables 1–5. Those were identified based on the consistent attitudes of

Table 2
A: Calculation of each parameter and classification in to four classes to evaluate IAT. B: Obtained classes according to the watersheds and calculated IAT. C: Extracted four classes of IAT as very high, high, moderate and low.

Watershed	Compactness Co-efficient	Lemniscate Coefficient (k)	Form Ratio	Basin Shape Index	Normalized Basin Asymmetry Factor	Hypsometric Integral (HI)	Elongation Ratio (Re)	Circularity Ratio (Rc)
1	1.889162322	1.964097364	0.39987707	1.387978142	7.876000678	0.307976503	0.713540279	0.280195689
2	1.77779771	1.471145513	0.533867991	1.036392634	8.839918972	0.190380952	0.824464925	0.316399155
3	2.082997189	1.840271853	0.426783412	1.174453395	19.55379427	0.217039806	0.737155327	0.230474368
4	2.312214105	2.255858507	0.348159026	1.76173913	10.64507715	0.527192365	0.665800431	0.187044054
5	2.277708304	2.122694027	0.140000335	1.955724225	14.66306108	0.344208978	0.425789345	0.162754173
6	1.939229896	2.987275967	0.262914277	2.213178295	3.336898061	0.256219172	0.578578548	0.265914123
7	2.020273435	2.120381095	0.370403934	1.580154861	8.867989087	0.257236488	0.686741098	0.245007677
8	1.83793788	2.998589827	0.261922285	2.051766139	22.58532287	0.328869855	0.577486011	0.296031784
9	2.855581348	7.392931515	0.106236274	3.143781452	10.37547271	0.396809143	0.367783006	0.122634009
10	2.251944545	4.709763864	0.166759422	2.716569767	23.81752359	0.301627866	0.460787229	0.197189877
11	2.688317702	5.312170836	0.14784869	2.705209657	3.368303308	0.416101041	0.433874357	0.138369004
12	2.145743641	4.330332726	0.181371167	3.236842105	24.4869634	0.268635339	0.480550868	0.217192254
13	2.038211568	3.866158979	0.203146716	2.949901121	5.262109451	0.40090294	0.508581017	0.24071407
14	2.079755795	4.248560211	0.184862038	3.119795471	20.61222037	0.247262427	0.485153436	0.231193337
15	2.154688957	4.581965328	0.171410616	4.087811271	10.65990776	0.279239835	0.467169091	0.215392625
16	2.139727602	5.31648741	0.147728649	4.505882353	6.91388037	0.272629124	0.433698185	0.218415282
17	2.497671762	5.192780688	0.151247963	4.152691968	17.49935923	0.268952645	0.438833738	0.160298431
18	2.417120975	5.842195044	0.134435344	4.696396396	25.11776766	0.278994017	0.413725199	0.171160374
19	1.906252086	3.643749247	0.215546528	2.692749462	25.89638308	0.342403852	0.52387269	0.275194238
20	2.26736741	5.503603755	0.14270604	3.484031936	0.368851965	0.428748487	0.426261806	0.19451639
21	1.870824648	1.800770754	0.436145189	1.18170581	9.258299253	0.287792886	0.745196464	0.285715521

A

(continued on next page)

Table 2 (*continued*)

Classification Range								
Classes	**Compactness Co-efficient(Cc)**	**Lemniscate Coefficient (k)**	**Form Ratio(Rf)**	**Basin Shape Index (Bs)**	**Normalized Basin Asymmetry Factor**	**Hypsometric Integral (HI)**	**Elongation Ratio (Re)**	**Circularity Ratio (Rc)**
Class 1	2.86 - 2.50	7.39 - 4.70	0.10 - 0.15	4.97 - 3.48	25.90 - 20.61	0.53 - 0.34	0.36 - 0.43	0.12 - 0.16
Class 2	2.49 - 2.15	4.69 - 3.64	0.16 - 0.21	3.47 - 2.21	20.60 - 10.66	0.33 - 0.28	0.44 - 0.52	0.17 - 0.20
Class 3	2.14 - 1.94	3.63 - 2.56	0.22 - 0.26	2.20 - 1.58	10.65 - 05.26	0.27 - 0.24	0.53 -0.58	0.21 - 0.24
Class 4	1.93 - 1.77	2.55 - 1.47	0.27 - 0.54	1.57 - 1.03	05.25 - 00.36	0.23 - 0.19	0.59 - 0.83	0.25 - 0.32

Watershed	**Compactness Co-efficient(Cc)**	**Lemniscate Coefficient (k)**	**Form Ratio(Rf)**	**Basin Shape Index(Bs)**	**Normalized Basin Asymmetry Factor**	**Hypsometric Integral (HI)**	**Elongation Ratio (Re)**	**Circularity Ratio (Rc)**	**Index of Active Tectonics(IAT)**
1	4	4	4	4	3	2	4	4	**3.625**
2	4	4	4	4	3	4	4	4	**3.875**
3	3	4	4	4	2	4	4	3	**3.5**
4	2	4	4	3	3	1	4	2	**2.875**
5	2	4	1	3	2	1	1	1	**1.875**
6	4	3	3	2	4	3	3	4	**3.25**
7	3	4	4	3	3	3	4	3	**3.375**
8	4	3	3	3	1	2	3	4	**2.875**
9	1	1	1	2	3	1	1	1	**1.375**
10	2	1	2	2	1	2	2	2	**1.75**
11	1	1	1	2	4	1	1	1	**1.5**
12	3	2	2	2	1	3	2	3	**2.25**
13	3	2	2	2	3	1	2	3	**2.25**
14	3	2	2	2	1	3	2	3	**2.25**
15	2	2	2	1	3	3	2	3	**2.25**
16	3	1	1	1	3	3	1	3	**2**
17	2	1	1	1	2	3	1	1	**1.5**
18	2	1	1	1	1	3	1	2	**1.5**
19	4	2	2	2	1	1	2	4	**2.25**
20	2	1	1	1	4	1	1	2	**1.625**
21	4	4	4	4	3	2	4	4	**3.625**

B

Classes	**Value**	**Tectonic Activeness**	**Watersheds**
Class 1	1.375 - 1.875	Very High	5,9,10,11,17,18,20
Class 2	1.876 - 2.250	High	12,13,14,15,16,19
Class 3	2.251 - 3.250	Moderate	4,6,8
Class 4	3.251 - 3.875	Low	1,2,3,7,21

C

few other faults in the nearby area and each having slickenlines with consistent attitudes. Slickenlines are visible only when observed closely. No displaced marker layers were found.

Paleostress analysis was performed on the collected attitudes of faults and lineations developed on them. We use T-TECTO (Studio X5) and Win_Tensor (4.0) software for paleostress analyses. The working principles of the software are available elsewhere (e.g., Vanik et al., 2018; Shaikh et al., 2020, Maurya et al., 2021; Goswami et al., 2022). We used two software programmes to cross-check results. This makes our analyses more reliable. We follow the convention, σ1 > σ2 > σ3, regarding the choice of symbols for maximum, intermediate and least principal stress axes, respectively.

4. Results

4.1. Morphotectonic analysis

The morphology of the study area is characterized by fluvial activities with distinct tectonic episodes. The 21 watersheds (Fig. 2A) are located in the hilly ranges of steep north-facing escarpment and gently south-dipping Mesozoic strata. The aspect slope map (Fig. 1A of Repository 1) displays the multi-slope directions followed by the rivers from the E-W elongated arc-shaped hilly patch dissected by several drainages. The average slope of the section varies from ~ 1 to > 12.6^0 (Fig. 1B of Repository 1).

A dendritic drainage pattern is well developed in watersheds 1 and 2. Regular high-angle joints and/or faults e.g., Banni Fault (NNW-SSE), Kutch Mainland Fault (W-E), Wagad Fault (E-W) and lineaments (probably) produced rectangular drainage patterns, which are distinct in watersheds 1, 3, 6 and 7. The complex structure with deformation of the Mid Jurassic-Lower Cretaceous uplift is accompanied by flexures and a second uplift that affected the Tertiary to Quaternary successions (Patil et al., 2013). It indicates major tectonic episodes resulting in a trellis drainage pattern (Flugel et al., 2015) near the Katrol Hill Fault (KHF) in the upper parts of watersheds 8–18 and 21. In watersheds 19 and 20, sub-parallel drainage was identified where channels joins ~ 40º around a recent sandy deposit (Fig. 2B). Rivers originated from the hilly elongated dome-shaped terrain with maximum elevation (Fig. 2A of Repository 1) and flow towards N, S, W, SW and NE. Compactness coefficient (Cc), form ratio (R_f) and lemniscate coefficient (k) denote the classes that include the watersheds (Fig. 2B-D of Repository 1).

Other geomorphic indicators viz., basin shape index (Bs), basin asymmetry factor (AF), hypsometric integral (HI), elongation ratio (Re)

Table 3
Details of calculated results and comparison of Vf, Smf, and IAT amongst class-1, class-2, class-3, and class-4.

Watersheds	Vf	Smf	IAT
Watershed 1	1.43	2.9	3.625
Watershed 2	1.61	2.85	3.875
Watershed 3	1.95	2.35	3.5
Watershed 4	1.16	1.46	2.875
Watershed 5	0.56	1.32	1.875
Watershed 6	1.26	2.61	3.25
Watershed 7	1.41	2.9	3.375
Watershed 8	1.66	1.85	2.875
Watershed 9	0.68	1.5	1.375
Watershed 10	0.52	1.77	1.75
Watershed 11	0.17	1.64	1.5
Watershed 12	1.03	1.53	2.25
Watershed 13	0.89	1.74	2.25
Watershed 14	0.79	1.59	2.25
Watershed 15	0.7	1.72	2.25
Watershed 16	0.83	1.26	2
Watershed 17	0.36	1.79	1.5
Watershed 18	0.7	1.88	1.5
Watershed 19	1.1	2.97	2.25
Watershed 20	0.71	2.55	1.625
Watershed 21	0.63	2.44	3.625

Colour Index	Class	Magnitude
	Class-1	Very high
	Class-2	High
	Class-3	Moderate
	Class-4	Low

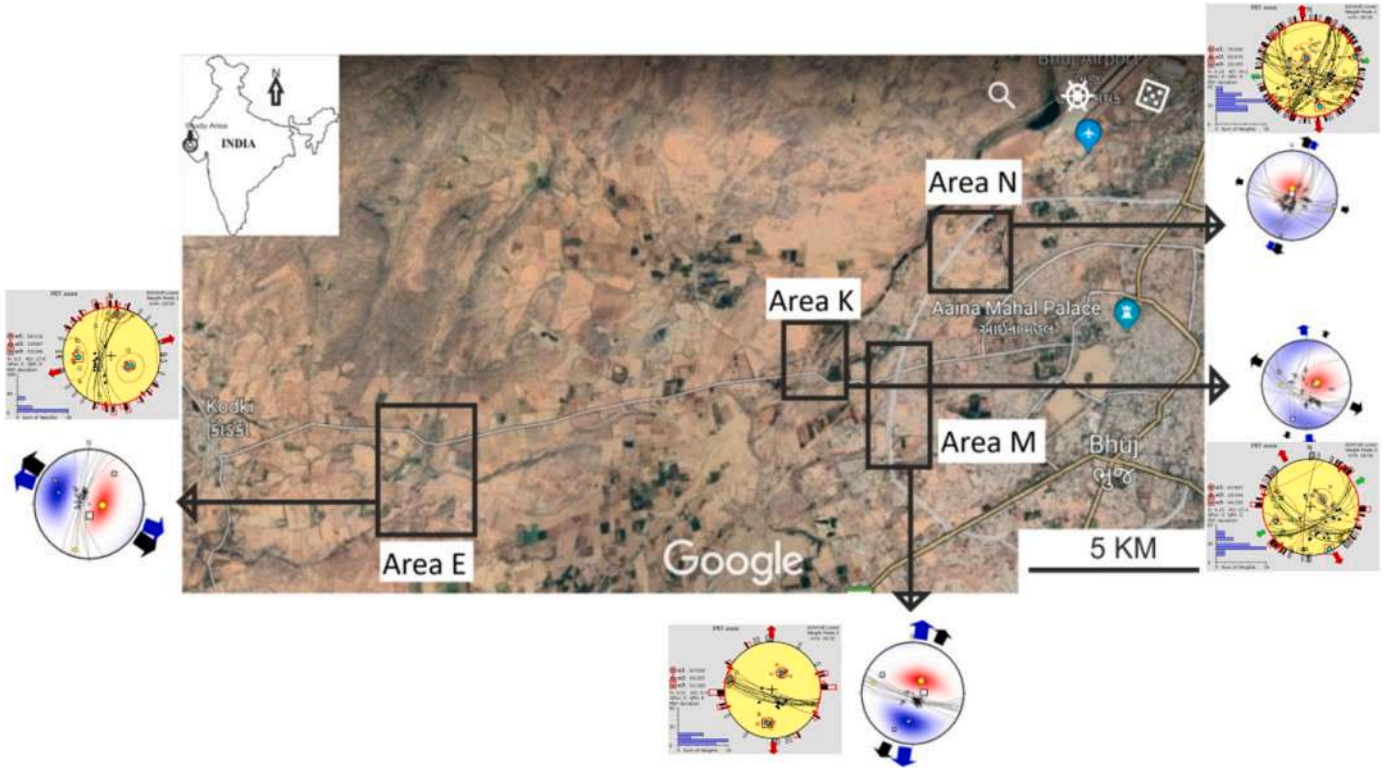

Fig. 3. Field locations E, K, M and N around Bhuj, on Google Earth Image. T-Tecto and Win_Tensor results at those locations are also presented. Great circles: input faults; three principal stress axes- yellow circles, the biggest intermediate and the smallest ones as σ_1, σ_2 and σ_3, respectively. Hollow squares: principle strain directions: biggest, intermediate and the smallest ones being ε_1, ε_2 and ε_3, respectively; blue patches: extensional field; red patches: compressive fields; Red and blue arrows: direction of compressive and tensile stresses, respectively. Black inward and outward arrows: direction of strain tensors. These tensors can be multi-directional representing several phases of faulting.

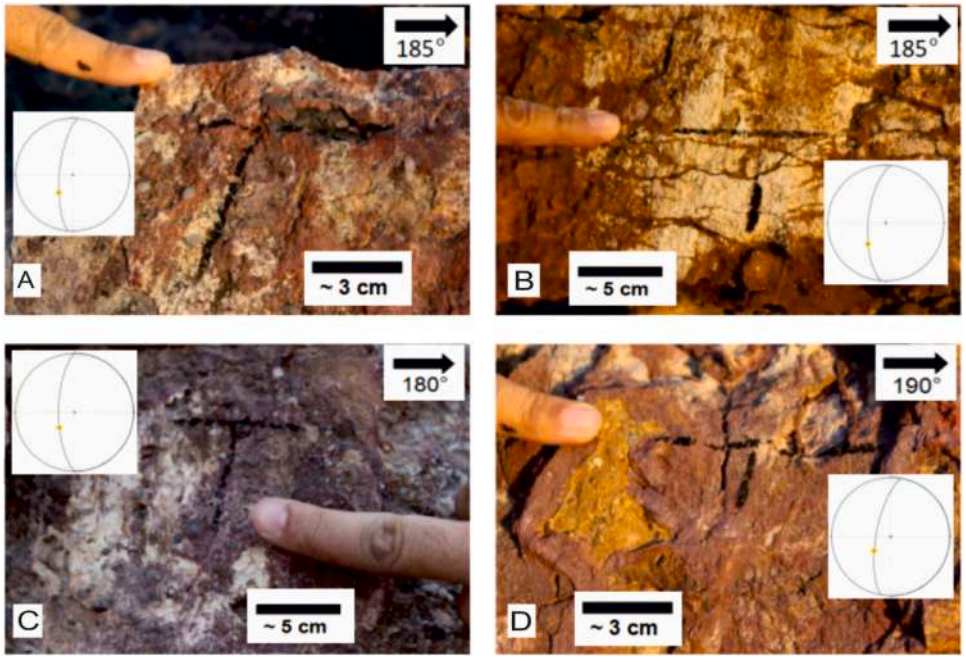

Fig. 4. Location E: Kodki road, western outskirts of Bhuj city. Inset: stereo plot: great circle - fault plane, yellow dot - slicken lines (Stereo net 10.4.0, Allmendinger et al., 2012). A. Sub-vertical fault plane (strike: 185°, dip: 71°, rake of slicken lines: 63°). B. Fault plane (strike: 185°, dip: 65°, rake of slicken lines: 59°). C. Oblique slicken lines on fault plane (strike: 180°, dip: 68°, rake of lineation: 69°). D. Partially eroded exposed fault plane (strike: 190°, dip: 70°) with clear-cut slicken lines with 67° rake.

and circularity ratio (Rc) have been considered and classified to indicate the tectonic activeness. There are five watersheds under class 1 (HI = 0.53–0.34**).** This is followed by four watersheds under class 2 (HI = 0.33–0.28), nine under class 3 (HI = 0.27–0.24) and three under class 4 (HI = 0.53–0.19) (Fig. 3A-E in Repository 1). Watersheds except 4, 9, 11, 13 and 19 belong to classes 2, 3 and 4, and they represent less tectonic activity.

The spatial distribution values specify the watersheds 5, 9, 10, 11, 17, 18 and 20 as highly active under class 1; watersheds 12–16 and 19 under high tectonic activity (class 2); watersheds 4, 6 and 8 under

Table 4
R-values define stress regime, as per Delvaux et al. (1997).

Stress regime	Vertical stress axis	R values
Radial Extension	σ_1	0–0.25
Pure Extension	σ_1	0.25–0.75
Transtension	σ_1	0.75–1
	Or σ_2	Or 1–0.75
Pure Strike Slip	σ_2	0.75–0.25
Transpression	σ_2	0.25–0
	Or σ_3	Or 0–0.25
Pure compression	σ_3	0.25–0.75
Radial Compression	σ_3	0.75–1

moderate scale (class 3); and watersheds 1, 2, 3, 7 and 21 as low active (class 4) (Fig. 2C; Table 2 A-C).

There are three main channels: the Khari, Pat and the Pur Rivers (Fig. 2D) in watershed 5. All flow towards the north and are characterized by deep vertical incision in the Khari river (Fig. 2E). The canyon (Fig. 2F) in the Khari River indicates the active tectonics near Bhuj. Fig. 2F1 represents recent activities of the Kutch Mainland Fault (Valdiya and Sanwal, 2017) that imposes more incision of the channel.

The calculated values of Smf and V_f have been used to classify the degree of active tectonics. A comparison with IAT ranges of different sectors discloses variable degrees of tectonic activities. The computed classes 1 and 2 have Smf within 1.6–1.53. Watersheds 4, 5 and 8–18 have Smf = 0.54–1.89. This indicates (very) active tectonic regime. These Smf values are strongly related to the IAT ranges where watersheds 4, 9–18 and 20 are under the very high and high ranges. The class 1 and 2 ranges of V_f are 0–0.6 and 0.61–1.21, respectively, and include the watersheds 4, 5 and 10–21. This reflects active tectonics associated with the KMF, Naira river Fault, KHF, Godpar Fakirwari Fault, Bhujpur Fault, Sandsra Dungar Fault etc. (plotted in Fig. 2c) created relatively narrow and deep valleys.

Formation of river terraces and their incision rates help to determine the uplift rate of the area. Along the central and eastern segment of KMF the rates of incision are 2–9 mm yr^{-1} and 2.3–10 mm yr^{-1} (Kothyari et al., 2022) that signify the low Smf, V_f and IAT values (under class1 and 2) of watershed 4,5 and 6. Near the Katrol hill zone, the average uplift rate is 0.8 mm yr^{-1} (Kothyari et al., 2022). Watersheds 9–20 are under the very high and high classes of IAT, V_f (watersheds10–21) and Smf (watersheds 8–18). The uplift rate is 3.1 mm yr^{-1} (Kothyari et al., 2022) in Khari watershed (watershed 5). In this watershed, Smf = 1.3, V_f = 0.56 and IAT = 1.8. All these values are under class 1 (very high tectonic activity) (Table 3).

4.2. Paleostress studies

Structural data were collected mostly from the rock exposures aside the Kodki road, Kalo Dungar road and the Airport Road passing through Bhuj. Fig. 3 in insets and Repository Tables 2–5 present the data collected for the paleostress analyses from different field locations. Brittle fault planes crop out in several sites. We are unable to map these faults since their trends and styles vary significantly. A single direction of extension is incompatible with the different fault-slip data that were recorded in the field. For a plausible explanation of such data, two directions of extension directions would be needed. The fault planes strike ~ N-S at locations K (Fig. 1 in Repository 2), and at location E (Fig. 2 in Repository 2) and ~ ENE at location N (Fig. 3 in Repository 2).

4.2.1. T-Tecto (Studio X5)

Paleostress analyses was performed based on field-data derived from faults (Fig. 4). T-TECTO provided the stress ratio [$R = (\sigma_2 - \sigma_3)(\sigma_1 - \sigma_3)^{-1}$] that constrains the shape of the stress ellipsoid (Žalohar and Vrabec, 2007). The highest possible value of R in different stress regimes is 1.0 for transtension and radial compression cases (Table 4). R also constrains the stress regime (Table 5).

4.2.2. Win_Tensor4.0 and comparison with T-Tecto

Principal stress axes σ_1, σ_2 and σ_3 are denoted by circle, triangle and square, respectively, in Win_Tensor. The planes of probable P, B and T axes deduced from the computed inversion analysis were also plotted.

The Win_Tensor results indicate that the stress regime is pure and extensive in areas E and M, whereas it is extensive in areas K and N. The σ_1 direction for areas E and K was ~ east and for areas M and N it was ~NNE. The σ_3 direction for area E was ~ west and for areas K, M and N it was ~ south. A dominantly extensional tectonic regime was revealed from the study locations with NW- and NNE-oriented extension directions, respectively. This means that in and around the Bhuj area, the W- to NE-oriented normal faults did not undergo reverse reactivation under current compressional stress regimes. Evidence of ~ N-S compression related to the India-Eurasia collision since ~ 55 Ma has been sparse from the study area (Fig. 3–8 in Repository 2).

5. Discussions

5.1. Geomorphic issue

Existence of faults were manifested as low Smf and V_f values that are comparable with low IAT range of watersheds 5, 9 and 10. The faults induced high uplift and straight mountain front. The low V_f values indicate vertical incision that justify the low IAT values connoting tectonic activeness.

The entire area is drained by rivers and their tributaries flowing S-N, N-S E-W and W-E from the anticline ridge forming a number of mesoscale watersheds. The SI value of tectonically active three watersheds indicate straight channel patterns, which are associated with vertical, valley side steep cutting corresponding to the least lateral erosion. Tectonic episodes reversed the stream gradients by bulging of the ground (Valdiya and Sanwal, 2017). Such uplifted section is accompanied by the high degree of drainage rejuvenation due to neotectonics (Valdiya and Sanwal, 2017). The main consequent streams in watersheds 2 and 3 near Bhuj show complex barbed pattern where tributaries join at hook-like junctions. It is accompanied by the E-W KHF, which is

Table 5
T-Tecto and Win_Tensor paleo stress results. Locations E to O are plotted in Fig. Y.

Locations	σ_1 (plunge/trend, in degree)		σ_2 (plunge/trend, in degree)		σ_3 (plunge/trend, in degree)	
	T-TECTO	Win_Tensor	T-TECTO	Win_Tensor	T-TECTO	Win_Tensor
E	61/96	54/114	6/197	13/007	27/290	33/268
K	61/81	67/057	29/269	23/248	3/177	4/156
M	57/34	57/028	12/285	09/285	30/188	31/189
N	71/002	70/339	6/111	02/075	19/203	20/165
O	56/349	74/333	3/254	03/073	33/162	16/164

intersected by N-S, NNE-SSW, and NNE-SSW lineaments/active faults (Valdiya and Sanwal, 2017).

With time drainage system were modified by several faults and re-framed the river course. These indicators justify the active tectonics and uplift of the area along with the neotectonic evidences e.g. strath terraces, knick points, laterally displaced crests. The study section of the KRB is characterized by several climatic as well as tectonic forces in the Late Quaternary (Maurya et al., 2003) under which topography got configured. This Quaternary tectonics was responsible for the 1821 and 1956 seismicities ($M > 5$) with the Kutch Mainland Fault Zone near Bhuj.

5.2. Paleostress analyses

The T-Tecto and Win-Tensor results from all the sectors match well. Most of the results show rather limited variations in plunge of the principal stress axes within 10^0 and a trend within $\sim$ 20–25^0. These discrepancies arose due to the different algorithms used in the two software (Dutta et al., 2019; Simon, 2019). For example, while T-Tecto uses the Gauss weighted right dihedral method, WinTensor applies the method the PBT axes. Limited variation in the paleosstress axes' attitudes deduced by different approaches give more confidence that the paleostress analyses were run correctly. Over a few km distance, principal paleostress axes orientations vary (e.g., the σ_3 direction in areas E, K and M; Fig. 3), and this is a common observation from many other terrains (e.g., Vanik et al., 2018; Kumar et al., 2022; Shaikh et al., 2022) (Table 5). Pealeostress directions do not necessarily link with the present-day stress system. This is true in terrains where a previously extensional regime is under compression, such as the KRB.

6. Conclusions

The IAT map of 21 watersheds in and around the Bhuj denotes that the watersheds 5, 9, 10, 11, 17, 18 and 20 are tectonically very active and come under class 1. It is accompanied by complex barbed and trellis drainage patterns, which indicate the area's tectonic interferences. Channels in some of these watersheds partially display complex barbed and trellis drainage patterns, which indicate a strong tectonic control.

Smf and V_f analyses disclose the active tectonic interferences both in the front area indicating uplift. The valley incision mechanism is characteristic in watershed 5. The active fault area between Dhrang and Khirsaia was the epicentre for the 2001 Bhuj earthquake ($M \sim 7.7$) and it belongs to the tectonically very active watershed 5.

Paleostress analyses indicate that NNE and NW-oriented extension acted around Bhuj producing normal faults. Sub-surface seismic image and ground penetrating radar (GPR) profile interpretation for hydrocarbon exploration in the area need to address the structures related to the paleostress regimes deciphered in this study.

Data Availability

Data will be made available on request.

Declaration of Competing Interest

We have strong conflict of interest with Arkprobho Biswas (Editorial board member on Results in Earth Sciences). Please do **not** give this article to him to handle ort review.

Acknowledgements

A part of this work was DM's M.Sc. thesis (Mayur, 2020) under SM's supervision. CPDA grant (IIT Bombay) to SM supported SM and DM to perform fieldwork. Md. Haroon Shaikh, Md Walid Omid, Nidhi Lohani and Aashu Pawar assisted in fieldwork. SM dedicates this article to Amy Shapiro (former worker in Elsevier, now with Frontiers) for her keen interest in seeing scientific publications going smoothly. We express gratitude to the Chief Editor Mimmo Palano and an anonymous reviewer for providing detail comments. Adrija Raha (Geography Department, Presidency University, Kolkata) assisted in finalizing a few figures.

Appendix A

Abbreviations	
AF	Basin asymmetry factor
Bs	Basin shape index
Cc	Compactness coefficient
HI	Hypsometric integral
IAT	Index of Active Tectonics
k	Lemniscate coefficient
KRB	Kutch Rift Basin
Rc	Circularity ratio
Re	Elongation ratio
Rf	Form ratio
Smf-	Mountain front sinuosity
V_f	Valley floor width height ratio

Appendix B. Supporting information

Supplementary data associated with this article can be found in the online version at doi:10.1016/j.rines.2023.100002.

References

Alapati, U., Jampani, M., Sukhtankar, R.K., 2019. Geomorphic response of the river basin drainage in seismically active regions of India. Environ. Earth Sci. 78, 1–5. https://doi.org/10.1007/s12665-019-8547-y

Allmendinger, R.W., Cardozo, N., Fisher, D.M., 2012. Structural Geology Algorithms: Vectors and Tensors. Cambridge University Press, The Edinburgh Building, Cambridge CB28RU, UK ISBN 978-1-107-01200-4.s.

Anand, A.K., Pradhan, S.P., 2019. Assessment of active tectonics from geomorphic indices and morphometric parameters in part of Ganga basin. J. Mount. Sci. 16, 1943–1961. https://doi.org/10.1007/s11629-018-5172-2

Biswas, S.K., Khattri, K.N., 2002. A geological study of earthquakes in Kachchh, Gujarat. J. Geol. Soc. India 60, 131–142.

Biswas, M., Gogoi, M.P., Mondal, B., Sivasankar, T., Mukherjee, S., Dasgupta, S., 2022. Geomorphic assessment of active tectonics in Jaisalmer basin (western Rajasthan, India. Geocarto Int. 1–32. https://doi.org/10.1080/10106049.2022.2066726

Biswas, M., Dhara, P., 2019. Correction to: Evolutionary characteristics of meander cut-off — A hydro-morphological study of the Jalangi River, West Bengal, India. Arab. J. Geosci. 12 (21), 1–21. https://doi.org/10.1007/s12517-019-4711-7

Biswas, M., Paul, A., 2021. Application of geomorphic indices to address the foreland Himalayan tectonics and landform deformation-Matiali-Chalsa-Baradighi recess, West Bengal, India. Quat. Int. 585, 3–14. https://doi.org/10.1016/j.quaint.2020.12.012

Brice J.C., 1964. Channel patterns and terraces of the Loup Rivers in Nebraska. Geological Survey Professional Paper. 422-D, Washington, D2–D41.
Bull, W.B., McFadden, L.D., 1977. Tectonic geomorphology north and south of the Garlock Fault, California. In: Doehring, D.O. (Ed.), Geomorphology in arid regions. Publications in Geomorphology. State University of New York, Binghampton. https://doi.org/10.1007/s13201-016-0524-y
Bull, W.B., 2007. Tectonic Geomorphology of Mountains: A New Approach to Paleoseismology. Wiley-Blackwell, Oxford, pp. 328.
Chandrasekhar, E., Mathew, G., Harinarayana, T., 2012. A new hypothesis for the deep subsurface structures near the Bhuj 2001 earthquake (Mw 7.6) hypocentre zone and its tectonic implications. Geophys. J. Int. 190 (2), 761–768. https://doi.org/10.1111/j.1365-246X.2012.05532.x
Chen, Y.C., Sung, Q., Cheng, K.Y., 2003. Along-strike variations of morphotectonic features in the Western Foothills of Taiwan: tectonic implications based on stream-gradient and hypsometric analysis. Geomorphology 56, 109–137. https://doi.org/10.1016/S0169-555X(03)00059-X
Chorley, R.J., 1957. Climate and morphometry. J. Geol. 65, 628–638. https://doi.org/10.1086/626468
Chowksey, V., Joshi, P., Maurya, D.M., Chamyal, L.S., 2011a. Ground penetrating radar characterization of fault-generated Quaternary colluvio-fluvial deposits along the seismically active Kachchh Mainland Fault, Western India. Curr. Sci. 100, 915–921. 〈https://www.jstor.org/stable/24076485〉.
Dasgupta, S., Biswas, M., Mukherjee, S., Chatterjee, R., 2022. Structural evolution and sediment depositional system along the transform margin- Palar-Pennar basin Indian east coast. J. Pet. Sci. Eng. 211, 110–155. https://doi.org/10.1016/j.petrol.2022.110155
Dasgupta, S., Mukherjee, S., 2017. Brittle shear tectonics in a narrow continental rift: asymmetric non-volcanic Barmer basin (Rajasthan, India). J. Geol. 125, 561–591. https://doi.org/10.1086/693095
Dasgupta, S., Mukherjee, S., 2019. Remote sensing in lineament identification: Examples from western India (Series Editor: Mukherjee S.) In: Billi, A., Fagereng, A. (Eds.), Problems and Solutions in Structural Geology and Vol. 5 Elsevier.
Delvaux, D., Moeys, R., Stapel, G., Petit, C., Levi, K., Miroshnichenko, A., Ruzhich, V., San'kov, V., 1997. Paleostress reconstructions and geodynamics of Baikal region, central Asia, Part 2. Cenozoic rifting. Tectonophysics 282, 1–38.
Dutta, D., Biswas, T., Mukherjee, S., 2019. Arc-parallel compression in the NW Himalaya: evidence from structural and palaeostress studies of brittle deformation from the clasts of the Upper Siwalik, Uttarakhand, India. J. Earth Syst. Sci. https://doi.org/10.1007/s12040-019-1138-1. 128-125.
Dwivedi, A.K., 2016. Petroleum exploration in india - a perspective and endeavours. Proc. India Nat. Sci. Acad. 82, 881–903. https://doi.org/10.16943/ptinsa/2016/48491
Flugel, J.T., Eckardt, D.F., Cotterill, P.D.F., 2015. The Present Day Drainage Patterns of the Congo River System and their Neogene Evolution. In: de Wit, M.J. (Ed.), Geology and Resource Potential of the Congo Basin. Regional Geology Reviews Springer-Verlag, pp. 315–337.
Goswami, T., Gogoi, M., Mahanta, B.N., Mukherjee, S., Saikia, H., Shaikh, M., Kalita, P., Baral, U., Sarmah, R., 2022. Brittle tectonics in the western Arunachal frontal fold belt, India: Change in stress regime from pre-collisional extension to collisional compression. Geol. J. https://doi.org/10.1002/gj.4514
Goswami, T.K., Mahanta, B.N., Mukherjee, S., Syngari, B.R., Sarmah, R.K., 2020. Orogen-transverse structures in the eastern Himalaya: Dextral Riedel shear along the Main Boundary Thrust in the Garu-Gensi area (Arunachal Pradesh, India), implication in hydrocarbon geosciences. Mar. Pet. Geol. 104–242. https://doi.org/10.1016/j.marpetgeo.2020.104242
Gupta, S., Biswas, M., 2022. Seismo-tectonic and morphological study of the north-east Himalaya. Geosci. J. 27, 1–21. https://doi.org/10.1007/s12303-022-0016-z
Hamdouni, R.E., Irigaray, C., Fernández, T., et al., 2008. Assessment of relative active tectonics, southwest border of the Sierra Nevada (southern Spain. Geomorphology 96, 150–173. https://doi.org/10.1016/j.geomorph.2007.08.004
Internet reference: 〈https://timesofindia.indiatimes.com/city/rajkot/petroleum-experts-mine-kutch-rocks/articleshow/74491585.cms〉 (Accessed on 14-Sept-2021).
Internet reference: 〈www.hydrocarbons-technology.com〉 (Accessed on 25-Sept-2022).
Iqbal, M., Sajjad, H., 2014. Prioritization based on morphometric analysis of Dudhganga Catchment, Kashmir Valley, India using remote sensing and geographical information system. Afr. J. Geo-Sci. Res. 2 (1), 1–6. 〈http://ajgr.rstpublishers.com/〉.
Jani, C., Kandregula, R., Bhosale, S., Chavan, A., Lakhote, A., et al., 2021. Delineation of tectonically active zones in the Island Belt Uplift region, Kachchh Basin, western India: a geomorphic and geodetic approach. Quat. Sci. Adv. 4, 100034. https://doi.org/10.1016/j.qsa.2021.100034
Kale, V.S., Sengupta, S., Achyuthan, H., Jaiswal, K.M., 2014. Tectonic controls upon Kaveri River drainage, cratonic Peninsular India: Inferences from longitudinal profiles, morphotectonic indices, hanging valleys and fluvial records. Geomorphology 227, 153–165. https://doi.org/10.1016/j.geomorph.2013.07.027
Kothyari, G., Kandregula, R., Dumka, R., Chauhan, G., Taloor, A., 2022. Quaternary tectonic history of seismically active intraplate Kachchh Rift Basin, western India: a review. Geodesy Geodyn. 13, 192–204. https://doi.org/10.1016/j.geog.2021.09.011
Kumar, A., Shaikh, M.A., Singh, S., Singh, T., Mukherjee, S., Singh, S., 2022. Active morphogenic faulting and paleostress analyses from the central Nahan salient, NW Siwalik Himalaya. Int. J. Earth Sci. 111, 1251–1267. https://doi.org/10.1007/s00531-022-02176-3
Kumar, D., Singh, S.D., Prajapati, K.S., Khan, I., Gautam, P.K., Vishawakarma, B., 2018. Morphometric parameters and neotectonics of Kalyani River Basin, Ganga Plain: a remote sensing and GIS approach. J. Geol. Soc. India 91, 679–686. https://doi.org/10.1007/s12594-018-0923-9
Lohani, N., Mukherjee, S., Singh, S., Pawar, A., Shaikh, M., 2022. Structural geological field guide: Bhuj area (Gujarat, India). In: Mukherjee, S. (Ed.), Structural Geology and Tectonics Field Guidebook Volume 2. Springer, pp. 227–250 ISBN: 978-3-031-19575-4.
Mayur, D., 2020. Tectonics of Kachchh basin based on field structural geological studies and paleostress analysis in Bhuj, Gujarat, India (Master Thesis). IISER,, Pune.
Maurya, D.M., Shaikh, M., Mukherjee, S., 2021. Comment on "Structural attributes and paleostress analysis of Quaternary landforms along the Vigodi Fault (VF) in Western Kachchh region. Quat. Int. 601, 143–147. https://doi.org/10.1016/j.quaint.2021.04.029
Maurya, D.M., Thakkar, M.G., Chamyal, L.S., 2003. Quaternary geology of the arid zone of Kachchh: terra incognita. Proc.-Indian Natl. Sci. Acad. Part A 69, 123–136.
Malik, J.N., Nakata, T., Sato, H., Imaizumi, T., Yoshioka, T., Philip, G., Mahajan, A.K., Karanth, R.V., 2001. January 26, 2001, the Republic Day (Bhuj) earthquake of Kachchh and active faults, Gujarat, western India. Active Fault Res. 20, 112–126. https://doi.org/10.11462/afr1985.2001.20_112
Morino, M., Malik, J.N., Mishra, P., Bhuiyan, C., Kaneko, F., 2008. Active fault traces along Bhuj Fault and Katrol Hill Fault, and trenching survey at Wandhay, Kachchh, Gujarat, India. J. Earth Syst. Sci. 117, 181–188. https://doi.org/10.1007/s12040-008-0022-1
Morisawa M. , 1985. Rivers, Longman, 1–222. ISBN 0–582-48982–2.
Mukherjee S., Dole G., Yatheesh V., Kale V. 2020. Tectonics of the Deccan trap: Focus on Indian Geoscientists' Contribution in the Last Four Years. In: Glimpse of Geoscience Researches in India. Proceedings of the Indian National Science Academy. 86, 237–244.
Mukherjee, S., 2018. Tectonics and Structural Geology: Indian Context. ISBN 978–3-319–99341-6.
Omid, M.W., Mukherjee, S., Dasgupta, S., 2021. Vein geometry (Bhuj, Gujarat, India). In: Mukherjee, S. (Ed.), Structural Geology and Tectonics Field Guidebook Volume 1. Springer Nature Switzerland AG, pp. 707–714 ISBN 978-3-030-60143-0.
Patidar, A.K., Maurya, D.M., Thakkar, M.G., Chamyal, L.S., 2007. Fluvial geomorphology and neotectonic activity based on field and GPR data, Katrol hill range, Kachchh, western India. Quat. Int. 159, 74–92.
Patil, D.J., Mani, D., Madhavi, T., Sudarshan, V., Srikarni, C., Kalpana, M.S., Dayal, A.M., 2013. Near surface hydrocarbon prospecting in Mesozoic Kutch sedimentary basin, Gujarat, Western India—A reconnaissance study using geochemical and isotopic approach. J. Pet. Sci. Eng. 108, 393–403. https://doi.org/10.1016/j.petrol.2013.05.002
Paul, A., Biswas, M., 2019. Changes in river bed terrain and its impact on flood propagation – a case study of River Jayanti, West Bengal, India. Geomat. Nat. Hazard. Risk 10, 1928–1947. https://doi.org/10.1080/19475705.2019.1650124
Prakash, K., Mohanty, T., Pati, J.K., et al., 2017. Morphotectonics of the Jamini River basin, Bundelkhand Craton, Central India; using remote sensing and GIS technique. Appl. Water Sci, 7, 3767–3782. https://doi.org/10.1007/s13201-016-0524-y
Sahu, S., Mohanty, S., 2021. Demarcation of zones of neotectonic activity around regional faults: morphometric analysis from the Wagad Highland, Kachchh, India. J, Earth Syst, Sci, 130, 219. https://doi.org/10.1007/s12040-021-01716-w
Schumm, S.A., 1956. The evolution of drainage systems and slopes in bad lands at Perth, Amboi, New Jersey. Geol. Soc. Am. Bullet. 63, 923–938. https://doi.org/10.1130/0016-7606(1956)67[597:EODSAS]2.0.CO;2
Sen, S., Kundan, A., Kalpande, V., Kumar, M., 2019. The present-day state of tectonic stress in the offshore Kutch-Saurashtra Basin, India. Mar. Pet. Geol. 102, 751–758. https://doi.org/10.1016/j.marpetgeo.2019.01.018
Seshu, D., Rao, P.R., Naganjaneyulu, K., 2016. Three-dimensional gravity modelling of Kutch region, India. J. Asian Earth Sci. 115, 16–28. https://doi.org/10.1016/j.jseaes.2015.09.015
Shaikh, M.A., Maurya, D.M., Mukherjee, S., Vanik, N.P., Padmalal, A., Chamyal, L.S., 2020. Tectonic evolution of the intra-uplift Vigodi-Gugriana-Khirasra-Netra Fault System in the seismically active Kachchh rift basin, India: implications for the western continental margin of the Indian plate. J. Struct. Geol. 140, 104–124. https://doi.org/10.1016/j.jsg.2020.104124
Shaikh, M.A., Patidar, A.K., Vanik, N.P., Padmalal, A., Tiwari, P., Mukherjee, S., Chamyal, L.S., 2022. Building tectonic framework of a blind active fault zone: quaternary deformation and near-surface fault zone stratigraphy inferred from field data and ground-penetrating radar imaging. J. Struct. Geol. 155, 104526. https://doi.org/10.1016/j.jsg.2022.104526
Simon, J.L., 2019. Forty years of paleostress analysis: has it attained maturity? J. Struct. Geol. 125, 124–133. https://doi.org/10.1016/j.jsg.2018.02.011
Singh, C.K., 2014. Active deformations extracted from drainage geomorphology; a case study from Southern Sonbhadra district, Central India. J. Geol. Soc. India 84 (5), 569–578. https://doi.org/10.1007/s12594-014-0164-5
Strahler, A.N., 1952. Hypsometric (area-altitude) analysis of erosional topography. Geol. Soc. Am. Bullet. 63, 1117–1142. https://doi.org/10.1130/0016-7606(1952)63[1117:HAAOET]2.0.CO;2
Thakkar, M.G., Maurya, D.M., Raj, R., Chamyal, L.S., 1999. Quaternary tectonic history and terrain evaluation of the area arund Bhuj, Mainland Kachchh, western India. J. Geol. Soc. India 53, 601–610.
Valdiya, K., Sanwal, J., 2017. Sabarmati Plain and Saurashtra–Kachchh Terranes. Dev. Earth Surf. Processes 207–221. https://doi.org/10.1016/b978-0-444-63971-4.00008-6
Vanik, N., Shaikh, H., Mukherjee, S., Maurya, D.M., Chamyal, L.S., 2018. Post-Deccan trap stress reorientation under transpression: Evidence from fault slip analyses from SW Saurashtra, western India. J. Geodyn. 121, 9–19. https://doi.org/10.1016/j.jog.2018.06.004
Withanage, W., Dayawansa, N.D.K., De Silva, R.P., 2014. Morphometric analysis of the Gal Oya River Basin using spatial data derived from GIS. Trop. Agric. Res. 26 (1), 175. https://doi.org/10.4038/tar.v26i1.8082